PAPER

Facile synthesis and characterization of magnesium and manganese mixed oxides for the efficient removal of tartrazine dye from aqueous media

Asma S. Al-Wasidi,[a] Fawaz A. Saad,[b] Alaa M. Munshi[b] and Ehab A. Abdelrahman [ID] *[cd]

Nanomaterials are the most effective class of substances for use as adsorbents in wastewater treatment. Hence, the current study involves the facile and low-cost synthesis of $MgMn_2O_4/Mn_2O_3$ and $MgMn_2O_4/Mn_2O_3/Mg_6MnO_8$ as novel nanostructures from mixed solutions of Mg(II) and Mn(II) ions using the Pechini sol–gel method. After that, the remaining powder was calcined at 500, 700, and 900 °C for 3 h; the products were designated as G500, G700, and G900, respectively. The G500 sample consists of $MgMn_2O_4$ and Mn_2O_3, while the G700 and G900 samples consist of $MgMn_2O_4$, Mg_6MnO_8, and Mn_2O_3. The synthesized nanostructures were characterized using several tools, such as X-ray diffraction (XRD), Fourier transform infrared spectroscopy (FT-IR), scanning electron microscopy (SEM), energy-dispersive X-ray spectroscopy (EDX), and N_2 adsorption/desorption analysis. The average crystallite size of the G500, G700, and G900 samples is 210.53, 95.27, and 83.43 nm, respectively. The SEM images showed that the G500 sample consists of square and rectangular bars with an average diameter of 3.18 μm. Also, the G700 and G900 samples consist of hexagonal, polyhedral, and irregular shapes with an average diameter of 1.12 and 0.54 μm, respectively. The synthesized nanostructures were further utilized as adsorbents for the efficient removal of tartrazine dye from aqueous media. The experimental data showed a good fit with the Langmuir isotherm and pseudo-first-order model. The maximum adsorption capacities of the G500, G700, and G900 adsorbents toward tartrazine dye are 328.95, 359.71, and 395.26 mg g^{-1}, respectively.

1. Introduction

The discovery of perfect water treatment methods is still a challenge for scientists, while industrialization and urbanization have a significant impact on living beings.[1–3] Azo dyes containing the –N=N– functional group are commonly utilized in the food processing, textile, and pharmaceutical industries. The release of these compounds into the environment causes water pollution. Azo dyes typically have a complex aromatic assembly and are resistant to light, oxidizers, and heat. These properties render these compounds non-degradable. Hence, they bioaccumulate in living organisms and cause severe disorders and diseases.[4,5] Tartrazine is a well-known food coloring found in jellies and drinks. Tartrazine is toxic and life-threatening because it can cause several diseases such as cancer

and asthma.[6] Consequently, such contaminants must be removed from the environment to decrease water pollution. The elimination of toxic dyes from wastewater is a crucial aspect that has attracted the interest of numerous research organizations worldwide. For wastewater treatment, different chemical and physical processes, like coagulation, sedimentation, ozonation, ultrasonication, photocatalysis, membrane separation, adsorbent polymer-based composites, strong photocatalysts, and adsorption, have been used alone or in combination.[7–15] However, adsorption is the most important method for removing non-degradable and persistent pollutants from wastewater because it is more economically and ecologically advantageous than other methods.[16–22] Nanomaterials had attracted considerable interest in the area of adsorption because of their unique characteristics of small size, enhanced porosity, and increased surface area.[23–32] The Pechini sol–gel method is preferable to other methods used to prepare metal oxide nanoparticles. This method is straightforward, requires low-cost materials, and controls the morphology and crystallite size of nanoparticles.[33–35] This method succeeded in preparing many nanomaterials such as α-Fe_2O_3, CuO/Li_3BO_3, $La_{0.8}Sr_{0.2}FeO_3$, Co_2SiO_4, $Bi_2ZnB_2O_7$, $CoAl_2O_4$, Gd_2CoMnO_6, and Co_3O_4.[36–43] However, the world needs more low-cost nanomaterials to get rid of the problem of water pollution. To

[a]Department of Chemistry, College of Science, Princess Nourah Bint Abdulrahman University, P. O. Box 84428, Riyadh 11671, Saudi Arabia

[b]Department of Chemistry, Faculty of Applied Sciences, Umm Al-Qura University, Makkah 21955, Saudi Arabia

[c]Department of Chemistry, College of Science, Imam Mohammad Ibn Saud Islamic University (IMSIU), Riyadh 11623, Saudi Arabia. E-mail: EAAAhmed@imamu.edu.sa; dr.ehabsaleh@yahoo.com

[d]Chemistry Department, Faculty of Science, Benha University, Benha 13518, Egypt

achieve this goal, our research group has synthesized $MgMn_2O_4/Mn_2O_3$ and $MgMn_2O_4/Mn_2O_3/Mg_6MnO_8$ as novel nanostructures using the Pechini sol–gel method. These nanostructures are considered novel because none of the scientists prepared them together through a single reaction. Also, the high surface area of these nanostructures makes them effective in removing contaminants from aqueous solutions. For the synthesis of these nanostructures, low-cost metal salts were used such as magnesium nitrate hexahydrate and manganese acetate tetrahydrate. The synthesized nanostructures were characterized using several tools such as XRD, FT-IR, SEM, EDX, and N_2 adsorption/desorption analyzer. The synthesized nanostructures were further utilized as adsorbents for the efficient removal of tartrazine dye from aqueous media. The experimental data of the adsorption process were collected and used to study reaction kinetics and adsorption isotherms.

2. Experimental

2.1. Materials

Magnesium nitrate hexahydrate ($Mg(NO_3)_2 \cdot 6H_2O$), manganese acetate tetrahydrate ($Mn(CH_3COO)_2 \cdot 4H_2O$), ethylene glycol ($C_2H_6O_2$), citric acid monohydrate ($C_6H_8O_7 \cdot H_2O$), sodium hydroxide (NaOH), tartrazine dye ($C_{16}H_9N_4Na_3O_9S_2$), hydrochloric acid (HCl), and potassium nitrate (KNO_3) were supplied by Sigma Aldrich Company and utilized as received without further purification.

2.2. Synthesis of nanostructures

6.28 g of $Mg(NO_3)_2 \cdot 6H_2O$ was dissolved in 50 mL of distilled water to obtain Mg(II) solution. Also, 6.00 g of $Mn(CH_3COO)_2 \cdot 4H_2O$ was dissolved in 50 mL of distilled water to obtain Mn(II) solution. 10.29 g of citric acid monohydrate was dissolved in 50 mL of distilled water. The Mg(II) solution was added to the Mn(II) solution then the citric acid solution was added with continuous stirring for 30 min. After that, 2 mL of ethylene glycol was added then the mixture was heated at 150 °C till dry. The remaining powder was calcinated at 500, 700, and 900 °C for 3 h then the products were encoded as G500, G700, and G900, respectively.

2.3. Instruments

The elements, morphology, and grain size of the G500, G700, and G900 samples were analyzed using SEM micrographs produced from a JSM-IT800 Schottky field emission scanning electron microscope (FE-SEM) which was attached to an energy-dispersive X-ray unit (EDX). The phase types and crystallite sizes of the G500, G700, and G900 samples were determined by X-ray diffraction (XRD) patterns acquired with a Bruker D_8 Advance X-ray diffractometer equipped with a CuK_α tube at 40 mA and 45 kV. The vibration modes of the G500, G700, and G900 samples were determined using a Nicolet iS50 Fourier transform infrared (FT-IR) spectrometer. The surface textures (average pore radius, BET surface area, and total pore volume) of the G500, G700, and G900 samples were analyzed using a Quantachrome TouchWin nitrogen gas sorption analyzer. The

concentration of the tartrazine dye was measured using a Shimadzu UV-1650 PC UV/Vis spectrophotometer. The maximum wavelength of the tartrazine dye is 428 nm.

2.4. Removal of the tartrazine dye from aqueous media

To attain the best conditions for the adsorption of the tartrazine dye, batch adsorption was utilized. Separately, 50 mg of the G500, G700, or G900 samples were added to 100 mL of 200 mg L^{-1} solutions of the tartrazine dye. Each mixture was stirred for a certain time. The solutions were then centrifuged to separate the adsorbents. The concentration of the tartrazine dye was measured at 428 nm using a Shimadzu UV-1650 PC UV/Vis spectrophotometer. The effects of pH (2–12), contact time (5–90 min), concentration of the tartrazine (150–300 mg L^{-1}), and temperature (298–328 K) were investigated.

Using eqn (1) and (2), the % removal (% R) of the tartrazine dye and the adsorption capacity (Q) of the adsorbents were calculated, respectively.

$$\% \ R = \frac{C_o - C_{eq}}{C_o} \times 100 \tag{1}$$

$$Q = C_o - C_{eq} \times \frac{V}{M} \tag{2}$$

where, C_o represents the initial concentration of the tartrazine dye (mg L^{-1}), C_{eq} represents the equilibrium concentration of the tartrazine dye (mg L^{-1}), V represents the volume of the tartrazine dye solution (L), and m represents the mass of adsorbents (g).

Point of zero charge (pH_{PZC}) of the G500, G700, and G900 adsorbents was determined using the batch method as described by Khalifa et al.[28] as the following; separately, 0.25 g of the G500, G700, or G900 samples were added to 50 mL of 0.02 M solutions of the KNO_3. The initial pH (pH_i) of the KNO_3 solutions was studied in the range from 2.5 to 11.5. Each mixture was stirred for 12 h. The final pH values (pH_f) were determined and plotted versus the initial pH values (pH_i). The pH_{PZC} is the pH_f level where a typical plateau was gotten.

3. Results and discussion

3.1. Characterization of the synthesized samples

Fig. 1A–C represents the XRD of the G500, G700, and G900 samples, respectively. The results showed that the G500 sample consists of magnesium manganese oxide ($MgMn_2O_4$ & JCPDS no. 00-0231-0392) and manganese oxide (Mn_2O_3 & JCPDS no. 01-080-3746). The peaks of $MgMn_2O_4$ in the G500 sample at $2\theta =$ 18.28°, 29.14°, 31.13°, 32.75°, 36.37°, 38.60°, 44.71°, 51.45°, 58.92°, 60.28°, 65.16°, 68.38°, 74.75°, and 78.23° are the results of (101), (112), (200), (103), (211), (004), (220), (105), (321), (224), (400), (206), (413), and (404) Miller indices, respectively. The peaks of Mn_2O_3 in the G500 sample at $2\theta =$ 26.52°, 40.23°, 43.08°, and 62.62° are the results of (220), (411), (420), and (620) Miller indices, respectively. The G700 sample consists of magnesium manganese oxide ($MgMn_2O_4$ & JCPDS no. 00-0231-0392), magnesium manganese oxide (Mg_6MnO_8 & JCPDS no. 01-089-4922), and manganese oxide (Mn_2O_3 & JCPDS no. 01-080-

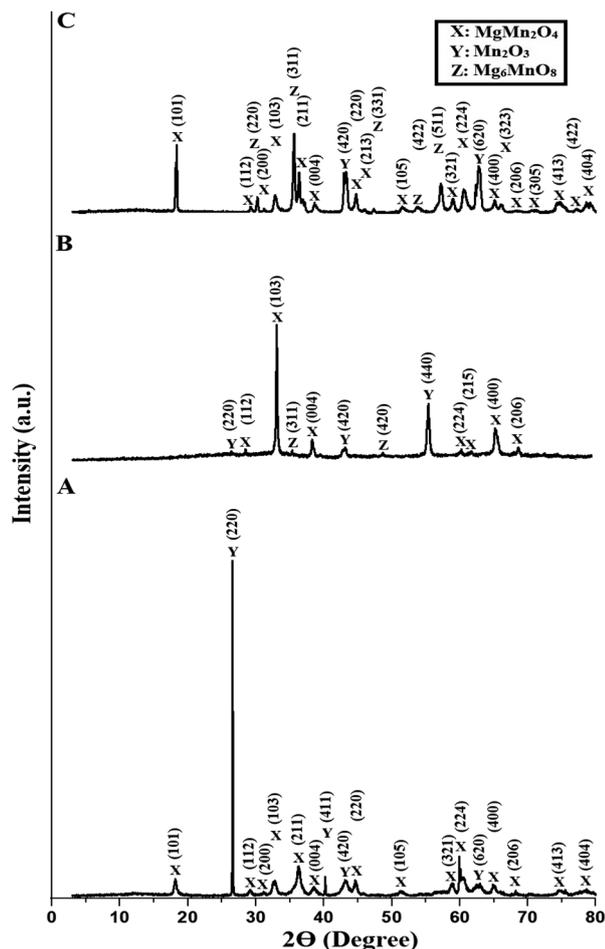Fig. 1   X-ray diffraction patterns of the G500 (A), G700 (B), and G900 (C) samples.

and 83.43 nm, respectively. A process related to the sol–gel method is the Pechini, or liquid mix, procedure. An aqueous solution of appropriate metal salts is mixed with an α-hydroxycarboxylic acid such as citric acid. Chelation, or the formation of complex ring-shaped products around the metal cations, takes place in the solution. A polyhydroxy alcohol such as ethylene glycol is then added, and the liquid is heated to 150 °C to allow the chelates to polymerize, or form large, cross-linked networks. As excess water is removed by heating, a solid polymeric resin result. Eventually, at still higher temperatures of 500–900 °C, the resin is decomposed or charred, and eventually mixed oxides are obtained. In the case of increasing the temperature, the organic substances were easily removed, and a small crystallite size of mixed oxides was obtained.[35]

Fig. 2   EDX patterns of the G500 (A), G700 (B), and G900 (C) samples.

3746). The peaks of $MgMn_2O_4$ in the G700 sample at $2\theta = 28.44°$, $33.07°$, $38.39°$, $60.23°$, $61.59°$, $65.90°$, and $69.15°$ are the results of (112), (103), (004), (224), (215), (400), and (206) Miller indices, respectively. The peaks of Mg_6MnO_8 in the G700 sample at $2\theta = 35.26°$ and $48.66°$ are the results of (311) and (420) Miller indices, respectively. The peaks of Mn_2O_3 in the G700 sample at $2\theta = 26.05°$, $42.80°$, and $55.39°$ are the results of (220), (420), and (440) Miller indices, respectively. The G900 sample consists of magnesium manganese oxide ($MgMn_2O_4$ & JCPDS no. 00-0231-0392), magnesium manganese oxide (Mg_6MnO_8 & JCPDS no. 01-089-4922), and manganese oxide (Mn_2O_3 & JCPDS no. 01-080-3746). The peaks of $MgMn_2O_4$ in the G900 sample at $2\theta = 18.27°$, $29.27°$, $31.26°$, $32.92°$, $36.24°$, $38.85°$, $44.78°$, $45.96°$, $51.66°$, $59.01°$, $60.67°$, $65.17°$, $66.12°$, $68.49°$, $70.86°$, $74.66°$, $77.26°$, and $78.68°$ are the results of (101), (112), (200), (103), (211), (004), (220), (213), (105), (321), (224), (400), (323), (206), (305), (413), (422), and (404) Miller indices, respectively. The peaks of Mg_6MnO_8 in the G900 sample at $2\theta = 30.35°$, $35.57°$, $47.31°$, and $53.94°$ are the results of (220), (311), (331), and (422) Miller indices, respectively. The peaks of Mn_2O_3 in the G900 sample at $2\theta = 43.08°$ and $62.62°$ are the results of (420) and (620) Miller indices, respectively. The average crystallite size of the G500, G700, and G900 samples is 210.53, 95.27,

Table 1 The EDX analysis of the G500, G700, and G900 samples

Sample	% C	% O	% Mg	% Mn
G500	6.19	19.33	22.48	52.00
G700	—	13.97	21.10	64.93
G900	—	17.87	29.63	52.50

Fig. 2A–C represents the EDX patterns of the G500, G700, and G900 samples, respectively. The results showed that the G500 sample consists of C, O, Mg, and Mn, as shown in Table 1. Also, the G700 and G900 samples consist of O, Mg, and Mn, as shown in Table 1. The presence of carbon in the G500 sample because 500 °C was insufficient for the complete liberation of organic substances. There was no carbon in the G700 and G900 samples because 700 and 900 °C were sufficient for complete liberation of organic substances.[35]
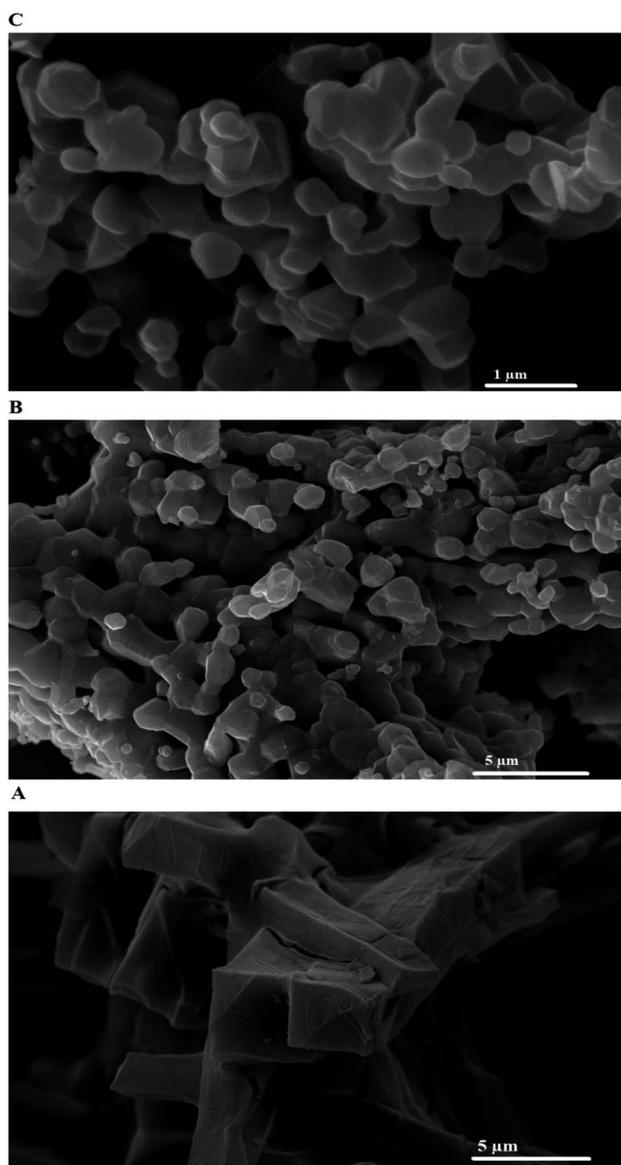
Fig. 3A–C represents the SEM images of the G500, G700, and G900 samples, respectively. The results showed that the G500 sample consists of square and rectangular bars with an average diameter of 3.18 μm. Also, the G700 and G900 samples consist of hexagonal, polyhedral, and irregular shapes with an average diameter of 1.12 and 0.54 μm, respectively. The temperature difference affects the shape of the obtained mixed oxides

Fig. 3 SEM images of the G500 (A), G700 (B), and G900 (C) samples.
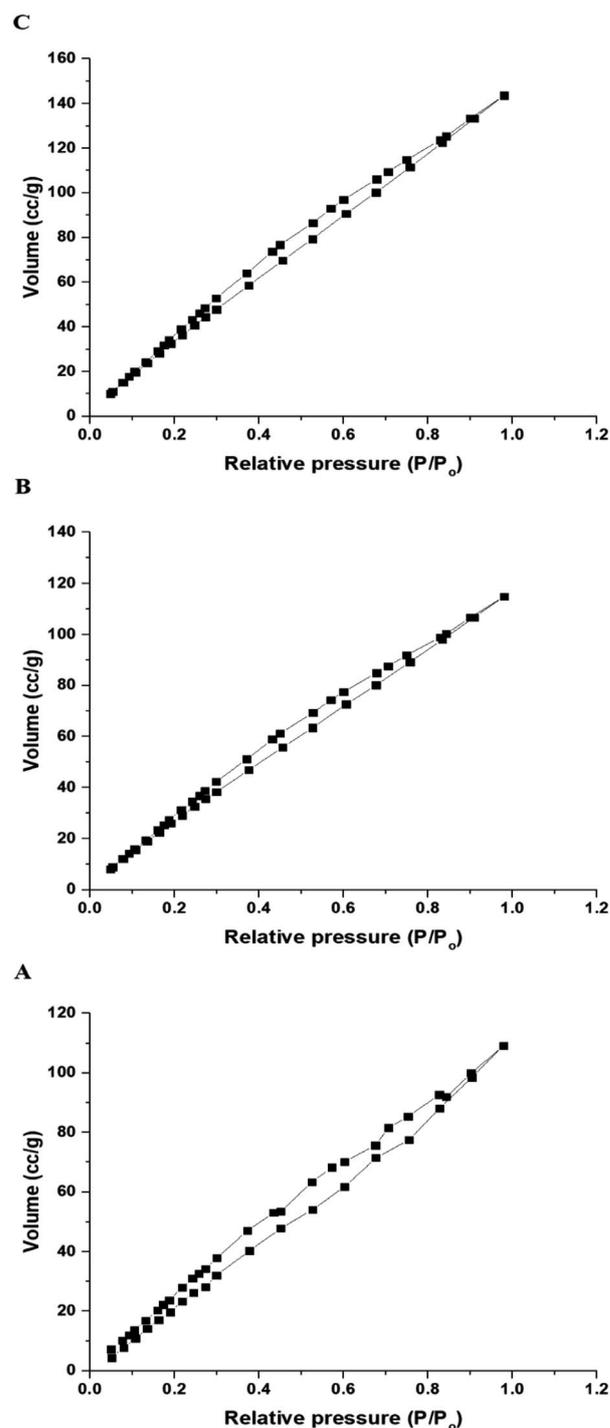
Fig. 4 N_2 adsorption/desorption isotherms of the G500 (A), G700 (B), and G900 (C) samples.

because the amount of gases released during the liberation of organic substances increases with increasing temperature.[35]

Fig. 4A–C represents the N_2 adsorption/desorption isotherms of the G500, G700, and G900 samples, respectively. The results showed that the isotherms of the G500, G700, and G900 samples belonged to type IV.[28] Also, the BET surface area and total pore volume increased in the following order; G500 < G700 < G900 as shown in Table 2. This observation can be explained using the average crystallite size because the BET surface area is inversely proportional to the average crystallite size. Besides, the average pore size of the G500, G700, and G900 samples was almost unaffected. This observation can be explained using the Pechini sol–gel method, which depends on the evolution of organic materials (citric acid monohydrate and ethylene glycol) from the inorganic/organic precursors to obtain the inorganic nanostructures. The calcination temperatures, which were used to remove these organic materials, affect the size and morphology of the nanostructures (*i.e.*, the BET surface area and total pore volume) without significantly affecting the average pore size.
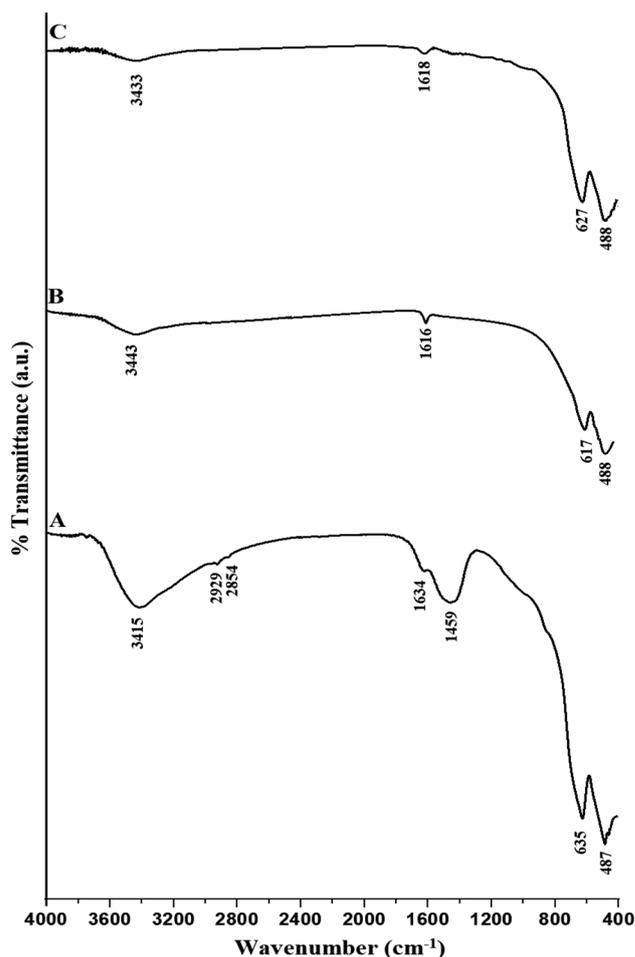
Fig. 5A–C represents the FT-IR spectra of the G500, G700, and G900 samples, respectively. The results showed that the bands, which were observed at 487, 488, and 488 cm^{-1} in the G500, G700, and G900 samples, are due to the stretching vibration of Mg–O, respectively. Also, the bands, which were observed at 635, 617, and 627 cm^{-1} in the G500, G700, and G900 samples, are due to the stretching vibration of Mn–O, respectively. Besides, the bands, which were observed at 1634, 1616, and 1618 cm^{-1} in the G500, G700, and G900 samples, are due to the bending vibration of OH, respectively. Moreover, the bands, which were observed at 3415, 3443, and 3433 cm^{-1} in the G500, G700, and G900 samples, are due to the stretching vibration of OH, respectively. The band, which was observed at 1459 cm^{-1} in the G500 sample, is due to the asymmetric bending vibration of C–OH of the remaining organic part. The bands, which were observed at 2854 and 2929 cm^{-1} in the G500 sample, are due to the stretching vibration of CH of the remaining organic part.[44–49]

3.2. Removal of tartrazine dye from aqueous media

3.2.1. Effect of pH. The effect of pH change (2–12) on the % removal of tartrazine dye and the adsorption capacity of the G500, G700, and G900 adsorbents was studied, and the results are shown in Fig. 6A and B, respectively. The tartrazine dye was observed to be removed most effectively under acidic conditions and least effectively under basic conditions. The maximum % removal of the tartrazine dye using the G500, G700, and G900 adsorbents was found to be 79.91%, 87.29%, and 97.37% at pH

Fig. 5 FT-IR spectra of the G500 (A), G700 (B), and G900 (C) samples.

= 2, respectively. Also, the maximum adsorption capacity of the G500, G700, and G900 adsorbents toward tartrazine dye was found to be 319.64 mg g^{-1}, 349.16 mg g^{-1}, and 389.46 mg g^{-1} at pH = 2, respectively. Therefore, other factors will be studied at pH 2. The pH$_{PZC}$ values of the G500, G700, and G900 adsorbents were found to be 6.50, 6.72, and 7.14, respectively as shown in Fig. 7. The results revealed that the G500, G700, and G900 adsorbents are positively charged at pH < pH$_{PZC}$. Hence, the % removal of tartrazine dye increased and reached a maximum level at pH = 2 due to the attraction between positively charged adsorbents and negatively charged tartrazine dye. Besides, the results revealed that the G500, G700, and G900 adsorbents are negatively charged at pH > pH$_{PZC}$. Hence, the % removal of tartrazine dye decreased and reached a minimum level at pH = 12 due to the repulsion between negatively charged adsorbents and negatively charged tartrazine dye.[28] The % removal or adsorption capacity increased in the following order; G500 < G700 < G900 because the BET surface area increases in the same order.

3.2.2. Effect of time. The effect of the time change (20–180) on the % removal of tartrazine dye and the adsorption capacity of the G500, G700, and G900 adsorbents was studied, and the results are shown in Fig. 8A and B, respectively. There was an

Table 2 The N_2 adsorption/desorption analysis of the G500, G700, and G900 samples

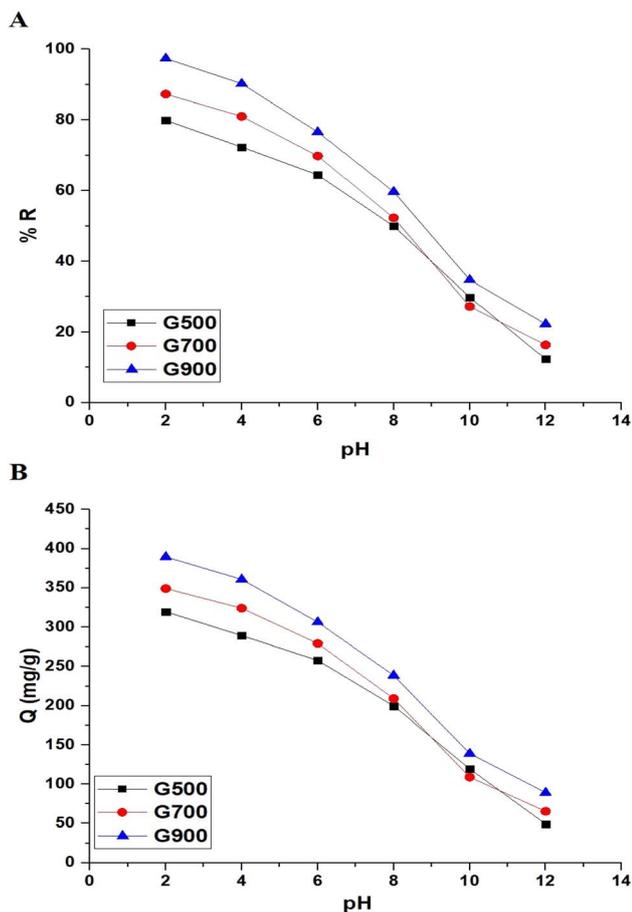| Sample	BET surface area (m^2 g^{-1})	Total pore volume (cm^3 g^{-1})	Average pore size (nm)
G500	204.32	0.1693	1.66
G700	216.46	0.1782	1.65
G900	270.57	0.2228	1.65

Fig. 6 The effect of pH change on the % removal of tartrazine dye (A) and the adsorption capacity of the G500, G700, and G900 adsorbents (B).
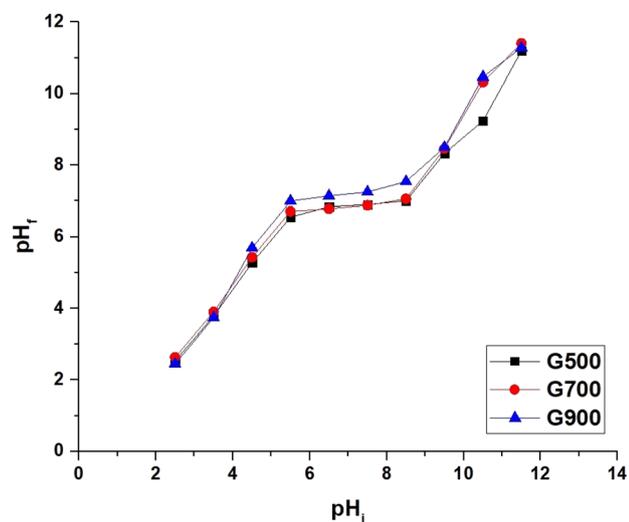

Fig. 8 The effect of the contact time on the % removal of tartrazine dye (A) and the adsorption capacity of the G500, G700, and G900 adsorbents (B).

Fig. 7 The pH$_{PZC}$ of the G500, G700, and G900 adsorbents.

increase in the % removal of tartrazine dye or adsorption capacity of the G500, G700, and G900 samples when the time increased from 20 min to 140 min due to the increase in the
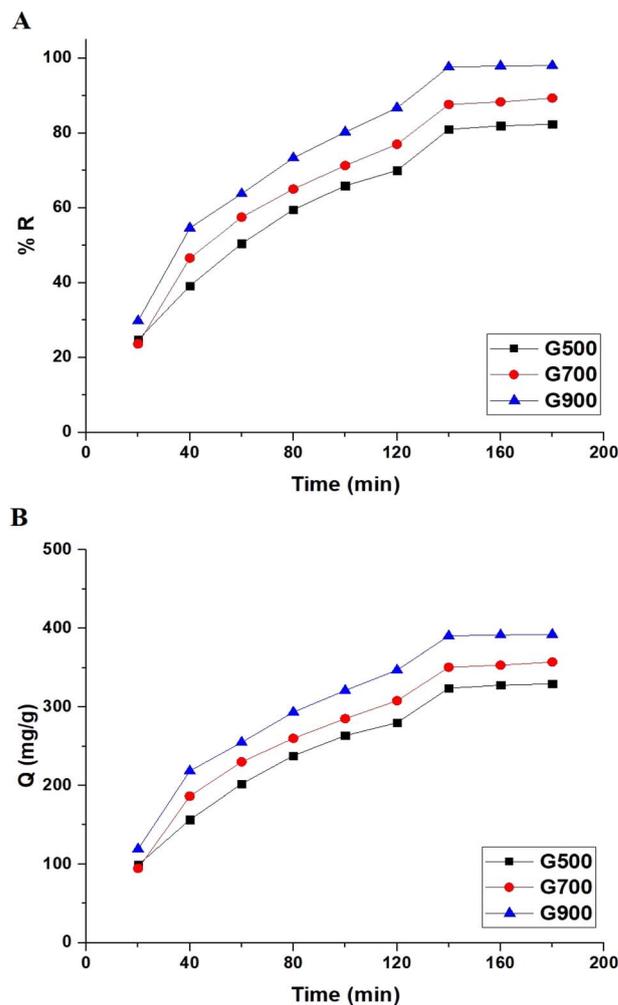
active centers. There is approximate stability in the % removal of tartrazine dye and adsorption capacity of the G500, G700, and G900 adsorbents when changing the time from 140 min to 180 min due to the saturation of active centers. The maximum % removal of the tartrazine dye using the G500, G700, and G900 adsorbents was found to be 81.00%, 87.68%, and 97.6% after 140 min, respectively. Also, the maximum adsorption capacity of the G500, G700, and G900 adsorbents toward tartrazine dye was found to be 324.00 mg g^{-1}, 350.70 mg g^{-1}, and 390.40 mg g^{-1} after 140 min, respectively. Therefore, other factors will be studied at 140 min.

The pseudo-first order (eqn (3)) and pseudo-second order (eqn (4)) were applied to the kinetics data of tartrazine dye adsorption on the G500, G700, and G900 adsorbents as shown in Fig. 9A and B, respectively.[28]

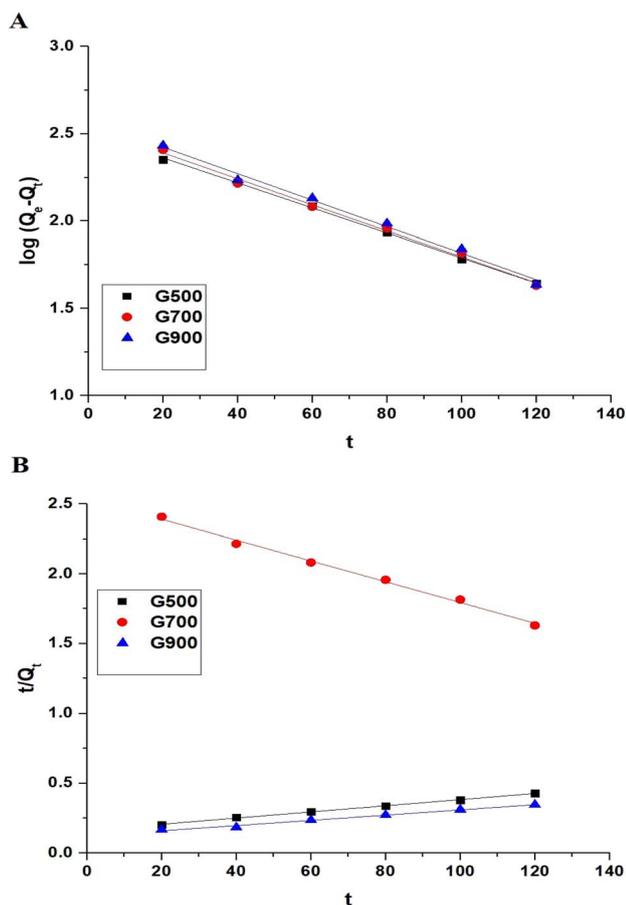$$\log(Q_e - Q_t) = \log Q_e - \frac{k_1}{2.303}t \qquad (3)$$

Fig. 9 The pseudo-first-order (A) and pseudo-second-order (B) models for the removal of tartrazine dye using the G500, G700, and G900 adsorbents.

Fig. 10 Temperature effects on tartrazine dye removal (A) and the adsorption capacities of the G500, G700, and G900 adsorbents (B).

Consequently, the experimental data showed a good fit with the pseudo-first-order model.

3.2.3. Effect of temperature. The effect of temperature change (298–328 K) on the % removal of tartrazine dye and the adsorption capacity of the G500, G700, and G900 adsorbents was studied, and the results are shown in Fig. 10A and B, respectively. There was a decrease in the % removal of tartrazine dye or adsorption capacity of the G500, G700, and G900 samples when the temperature increased from 298 K to 328 K. Therefore, other factors will be studied at 298 K.

The effect of temperature on the removal of tartrazine dye using the G500, G700, and G900 adsorbents can be represented by determining the thermodynamic parameters such as change in free energy ($\Delta G°$, kJ mol^{-1}), change in entropy ($\Delta S°$, kJ mol^{-1} K^{-1}), and change in enthalpy ($\Delta H°$, kJ mol^{-1}) using eqn (5)–(7).[28]

$$\frac{t}{Q_t} = \frac{1}{k_2 Q_e^2} + \frac{1}{Q_e} t \qquad (4)$$

where, Q_t is the amount of tartrazine dye adsorbed at time t (mg g^{-1}), Q_e is the adsorption capacity of the G500, G700, and G900 adsorbents at equilibrium (mg g^{-1}), k_1 is the rate constant for the pseudo-first-order model (min^{-1}), and k_2 is the rate constant for the pseudo-second-order model (g mg^{-1} min^{-1}). Table 3 depicts the kinetic parameters for the removal of tartrazine dye using the G500, G700, and G900 adsorbents. The correlation coefficient (R^2) values were used to select the best-fitting model. Table 3 reveals that the R^2 values derived from the pseudo-second-order model are less than those derived from the pseudo-first-order model.
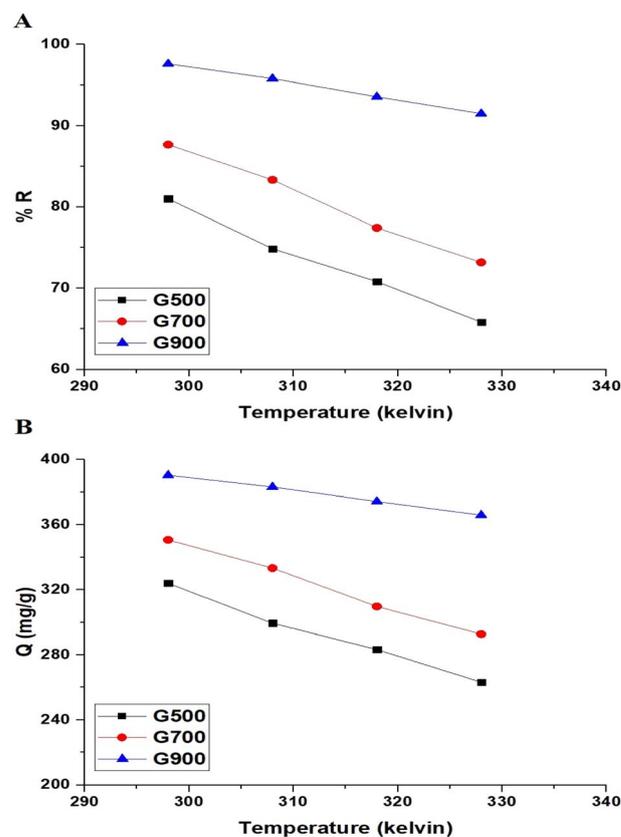
Table 3 The kinetic parameters for the removal of tartrazine dye using the G500, G700, and G900 adsorbents

Adsorbents	Pseudo-first-order			Pseudo-second-order		
	Q_e (mg g^{-1})	k_1 (min^{-1})	R^2	Q_e (mg g^{-1})	k_2 (g mg^{-1} min^{-1})	R^2
G500	320.52	0.0165	0.9989	452.49	3.015×10^{-5}	0.9975
G700	346.54	0.0172	0.9936	520.83	2.38×10^{-5}	0.9645
G900	376.13	0.0175	0.9900	534.76	2.88×10^{-5}	0.9867

$$\ln K_{\mathrm{d}} = \frac{\Delta S^{\circ}}{R} - \frac{\Delta H^{\circ}}{RT} \qquad (5)$$

$$\Delta G^{\circ} = \Delta H^{\circ} - T\Delta S^{\circ} \qquad (6)$$

$$K_{\mathrm{d}} = \frac{Q_{\mathrm{e}}}{C_{\mathrm{eq}}} \qquad (7)$$

where, T is the adsorption temperature (K), K_{d} is the distribution constant (L g^{-1}), and R is the gas constant (kJ mol^{-1} kelvin^{-1}). By plotting the values of $\ln K_{\mathrm{d}}$ against $1/T$, the values of ΔS° and ΔH° can be calculated using the intercept and slope, as displayed in Fig. 11 and Table 4. Additionally, ΔG° values were calculated based on ΔH° and ΔS° values, as displayed in Table 4. The negative sign of the ΔH° values reveals that the removal of tartrazine dye is exothermic.[28] In addition, the values of ΔH° are less than 40 kJ mol^{-1}, which indicate the physical nature of the adsorption. The positive value of (ΔS°) indicates greater randomization at the solid/solution interface after the removal of the tartrazine dye using the G500, G700, and G900 adsorbents. The negative values of ΔG° indicated the spontaneous nature of the removal of tartrazine dye.

3.2.4. Effect of concentration. The effect of the concentration change (150–300) on the % removal of tartrazine dye and the adsorption capacity of the G500, G700, and G900 adsorbents was studied, and the results are shown in Fig. 12A and B,
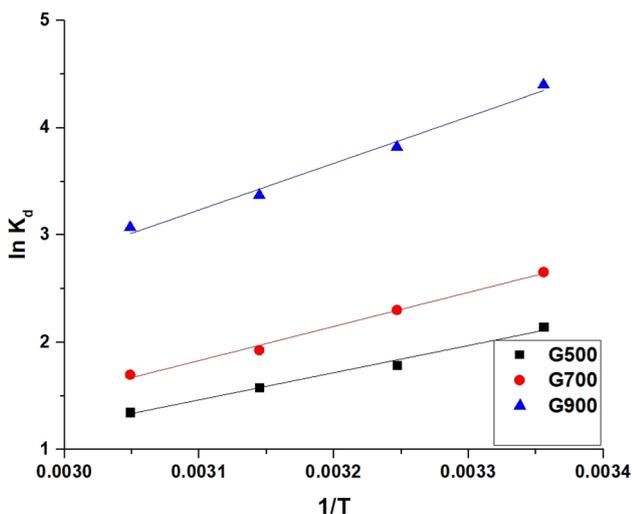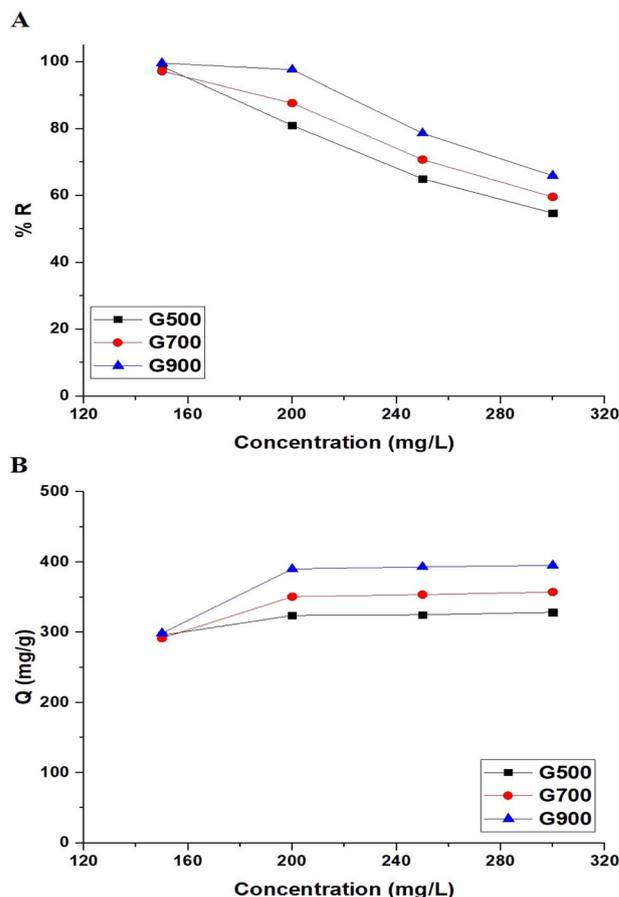
Fig. 12 The effect of concentration on the % removal of tartrazine dye (A) and the adsorption capacity of the G500, G700, and G900 adsorbents (B).

respectively. There was a decrease in the % removal of tartrazine dye and an increase in the adsorption capacity of the G500, G700, and G900 samples when the concentration increased from 150 mg L^{-1} to 300 mg L^{-1}.

The Langmuir (eqn (8)) and Freundlich (eqn (9)) were applied to the equilibrium data of tartrazine dye adsorption on the G500, G700, and G900 adsorbents as shown in Fig. 13A and B, respectively.[28]

$$\frac{C_{\mathrm{eq}}}{Q_{\mathrm{e}}} = \frac{1}{k_{\mathrm{L}} Q_{\mathrm{max}}} + \frac{C_{\mathrm{eq}}}{Q_{\mathrm{max}}} \qquad (8)$$

$$\ln Q_{\mathrm{e}} = \ln k_{\mathrm{F}} + \frac{1}{n}\ln C_{\mathrm{eq}} \qquad (9)$$

Fig. 11 The plot of $\ln K_{\mathrm{d}}$ against $1/T$ for the removal of tartrazine dye using the G500, G700, and G900 adsorbents.

Table 4 The values of ΔS°, ΔG°, and ΔH° for the removal of tartrazine dye using the G500, G700, and G900 adsorbents

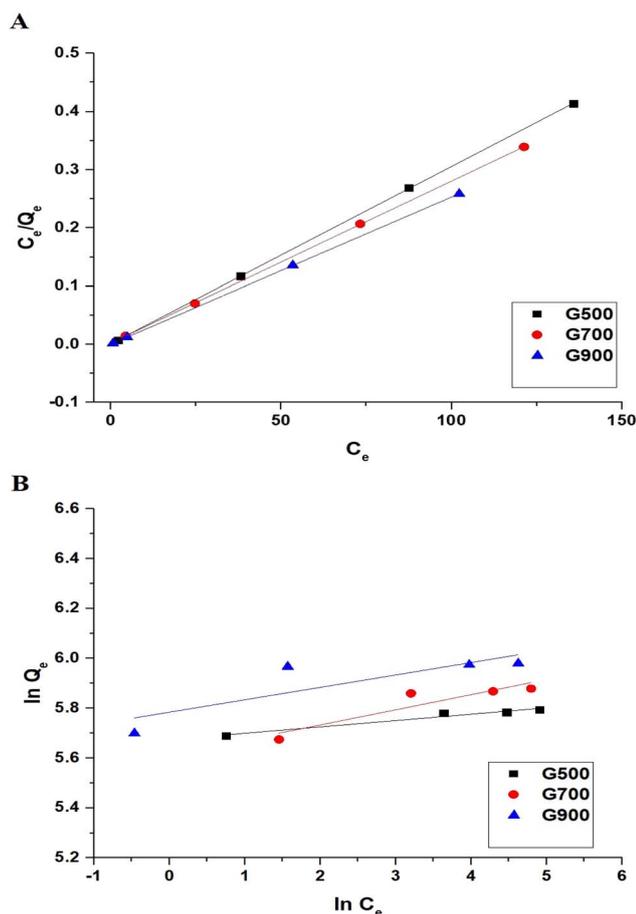| Adsorbent	ΔH° (kJ mol^{-1})	ΔS° (kJ mol^{-1} K^{-1})	ΔG° (kJ mol^{-1})			
			298	308	318	328
G500	−21.22	0.0536	−37.18	−37.72	−38.25	−38.79
G700	−26.60	0.0672	−46.62	−47.29	−47.96	−48.63
G900	−36.38	0.0857	−61.93	−62.78	−63.64	−64.49

Fig. 13 The Langmuir (A) and Freundlich (B) isotherms for the removal of tartrazine dye using the G500, G700, and G900 adsorbents.

where, k_L is the equilibrium constant of the Langmuir isotherm ($L\ mg^{-1}$), Q_{max} is the maximum adsorption capacity of the Langmuir isotherm ($mg\ g^{-1}$), k_F is the equilibrium constant of the Freundlich isotherm ($mg\ g^{-1}$)($L\ mg^{-1}$)$^{1/n}$, and $1/n$ is the heterogeneity constant. The Freundlich isotherm can be used to calculate the Q_{max} using eqn (10).[28]

$$Q_{max} = k_F(C_o^{1/n}) \tag{10}$$

Table 5 depicts the equilibrium parameters for the removal of tartrazine dye using the G500, G700, and G900 adsorbents. The correlation coefficient (R^2) values were used to select the best-fitting isotherm. Table 5 reveals that the R^2 values derived from the Freundlich isotherm are less than those derived from the Langmuir isotherm. Consequently, the experimental data showed a good fit with the Langmuir isotherm.

The maximum adsorption capacities of the G500, G700, and G900 adsorbents toward tartrazine dye are 328.95, 359.71, and 395.26 $mg\ g^{-1}$, respectively. The maximum adsorption capacities of the G500, G700, and G900 adsorbents toward tartrazine dye are greater than those of other adsorbents in the literature as shown in Table 6.[50–53]

3.2.5. Regeneration and reusability study. To regenerate the adsorbents, tartrazine dye is completely removed from the surface of the adsorbents by stirring the adsorbents loaded with dye in 50 mL of 4 M NaOH for 30 min. Afterward, the regenerated adsorbents were used for the removal of tartrazine dye for four consecutive cycles as previously described in the experimental part. The adsorption capacity of tartrazine dye using the G500, G700, and G900 adsorbents did not change significantly as shown in Fig. 14A–C, respectively.

Table 5 The equilibrium parameters for the removal of tartrazine dye using the G500, G700, and G900 adsorbents

Adsorbent	Langmuir isotherm			Freundlich isotherm		
	Q_{max} ($mg\ g^{-1}$)	k_L ($L\ mg^{-1}$)	R^2	Q_{max} ($mg\ g^{-1}$)	k_F ($mg\ g^{-1}$)($L\ mg^{-1}$)$^{1/n}$	R^2
G500	328.95	2.1111	0.9999	333.45	291.2174	0.9469
G700	359.71	1.0988	0.9999	377.60	273.4667	0.7837
G900	395.26	5.5763	0.9999	423.41	325.1966	0.5745

Table 6 Comparison between the adsorption capacities of the G500–G700 adsorbents and those of various adsorbents

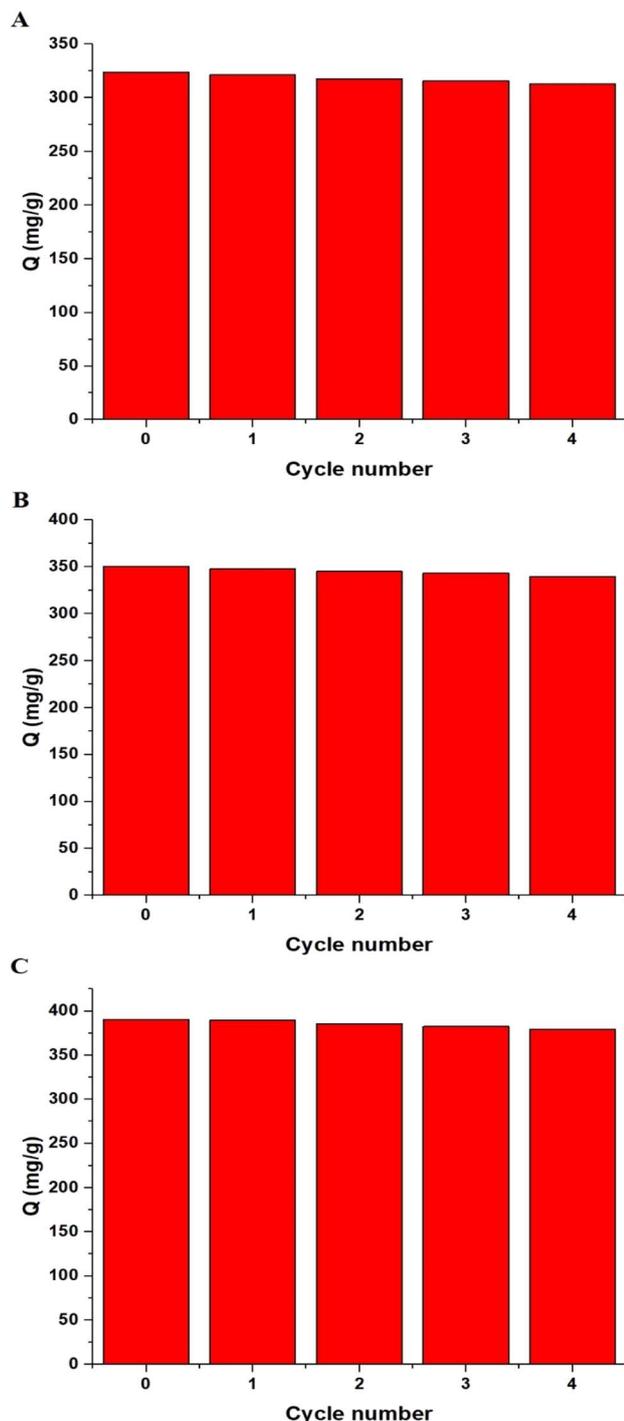| Adsorbent	Q_{max} ($mg\ g^{-1}$)	Ref.
Ni–Ag bimetallic nanoparticles supported on reduced graphene oxide	26.31	50
Iron oxide nanoparticles	59.79	51
Carbon-magnetic layered double hydroxide	52.30	52
Polypyrrole coated tenorite nanoparticles	42.50	52
ZnS/CuO/carbon nanotube	183.50	53
G500	328.95	This study
G700	359.71	This study
G900	395.26	This study

Fig. 14 The plot of the adsorption capacities of the G500 (A), G700 (B), and G900 (C) samples *versus* cycle number.

4. Conclusions

The current study includes the simple and inexpensive synthesis of $MgMn_2O_4/Mn_2O_3$ and $MgMn_2O_4/Mn_2O_3/Mg_6MnO_8$ as novel nanostructures from mixed solutions of Mn(II) and Mg(II) ions utilizing the Pechini sol–gel method. Following this, the remaining powder was calcinated for 3 h at 500, 700, and 900 °C, and the resulting products were labeled G500, G700, and G900, respectively. The synthesized nanostructures were utilized for the efficient removal of tartrazine dye from aqueous media. The maximum adsorption capacities of the G500, G700, and G900 adsorbents toward tartrazine dye are 328.95, 359.71, and 395.26 mg g^{-1}, respectively.

Conflicts of interest

The authors confirm that there is no conflict of interest for this paper.

Acknowledgements

References

1 A. Kausar, S. T. Zohra, S. Ijaz, M. Iqbal, J. Iqbal, I. Bibi, S. Nouren, N. El Messaoudi and A. Nazir, *Int. J. Biol. Macromol.*, 2022, **224**, 1337–1355.

2 M. Bilal, I. Ihsanullah, M. U. Hassan Shah, A. V. Bhaskar Reddy and T. M. Aminabhavi, *J. Environ. Manage.*, 2022, **321**, 115981.

3 G. Sriram, A. Bendre, E. Mariappan, T. Altalhi, M. Kigga, Y. C. Ching, H. Y. Jung, B. Bhaduri and M. Kurkuri, *Sustain. Mater. Technol.*, 2022, **31**, e00378.

4 Y. Dadban Shahamat, M. Masihpour, P. Borghei and S. Hoda Rahmati, *Inorg. Chem. Commun.*, 2022, **143**, 109785.

5 O. Moradi, A. Pudineh and S. Sedaghat, *Food Chem. Toxicol.*, 2022, **169**, 113412.

6 H. Singh, A. Goyal, S. K. Bhardwaj, M. Khatri and N. Bhardwaj, *Mater. Sci. Eng. B: Solid-State Mater. Adv. Technol.*, 2023, **288**, 116165.

7 A. Spoială, C. I. Ilie, G. Dolete, A. M. Croitoru, V. A. Surdu, R. D. Trușcă, L. Motelica, O. C. Oprea, D. Ficai, A. Ficai, E. Andronescu and L. M. Dițu, *Membranes*, 2022, **12**, 804.

8 L. Motelica, B. S. Vasile, A. Ficai, A. V. Surdu, D. Ficai, O. C. Oprea, E. Andronescu, D. C. Jinga and A. M. Holban, *Pharmaceutics*, 2022, **14**, 2842.

9 J. Lu, X. Huang, Z. Zhang, H. Pang, K. Chen, H. Xia, Y. Sui, R. Chen and Z. Zhao, *Water Res.*, 2022, **226**, 119245.

10 Y. Li, Y. Wang, J. Jin, Z. Tian, W. Yang, N. J. D. Graham and Z. Yang, *Water Res.*, 2023, **229**, 119447.

11 K. Li, W. Xu, G. Wen, Z. Zhou, M. Han, S. Zhang and T. Huang, *Chemosphere*, 2022, **308**, 136520.

12 Q. Qin, J. Li, H. Jia and J. Wang, *Water Res.*, 2022, **224**, 119109.

13 L. D. Tijing, J. R. C. Dizon, I. Ibrahim, A. R. N. Nisay, H. K. Shon and R. C. Advincula, *Appl. Mater. Today*, 2020, **18**, 100486.

14 M. A. Abdelwahab, S. M. El Rayes, M. M. Kamel and E. A. Abdelrahman, *Int. J. Environ. Anal. Chem.*, 2022, DOI: **10.1080/03067319.2022.2100260**.

15 E. A. Abdelrahman, R. M. Hegazey, S. H. Ismail, H. H. El-Feky, A. M. Khedr, M. Khairy and A. M. Ammar, *Arabian J. Chem.*, 2022, **15**, 104372.

16 A. S. Al-Wasidi, A. M. Naglah, F. A. Saad and E. A. Abdelrahman, *Arabian J. Chem.*, 2022, **15**, 104010.

17 A. S. Al-Wasidi, H. S. AlSalem, A. F. Alshalawi, A. M. Naglah, A. Al-Anwar and E. A. Abdelrahman, *Arabian J. Chem.*, 2022, **15**, 104113.

18 A. S. Al-Wasidi, A. M. Naglah, F. A. Saad and E. A. Abdelrahman, *Arabian J. Chem.*, 2022, **15**, 104178.

19 H. M. Gad, S. M. El Rayes and E. A. Abdelrahman, *RSC Adv.*, 2022, **12**, 19209.

20 D. Mei, L. Liu and B. Yan, *Coord. Chem. Rev.*, 2023, **475**, 214917.

21 Y. Zhang, J. Luo, H. Zhang, T. Li, H. Xu, Y. Sun, X. Gu, X. Hu and B. Gao, *Sci. Total Environ.*, 2022, **852**, 158201.

22 L. Pellenz, L. J. S. da Silva, L. P. Mazur, G. M. de Figueiredo, F. H. Borba, A. A. Ulson de Souza, S. M. A. Guelli Ulson de Souza and A. da Silva, *J. Water Process. Eng.*, 2022, **48**, 102873.

23 E. A. Abdelrahman, *J. Mol. Liq.*, 2018, **253**, 72–82.

24 E. A. Abdelrahman, D. A. Tolan and M. Y. Nassar, *J. Inorg. Organomet. Polym. Mater.*, 2019, **29**, 229–247.

25 E. A. Abdelrahman and R. M. Hegazey, *Microchem. J.*, 2019, **145**, 18–25.

26 E. A. Abdelrahman and R. M. Hegazey, *Composites, Part B*, 2019, **166**, 382–400.

27 E. A. Abdelrahman, R. M. Hegazey and R. E. El-Azabawy, *J. Mater. Res. Technol.*, 2019, **8**, 5301–5313.

28 M. E. Khalifa, E. A. Abdelrahman, M. M. Hassanien and W. A. Ibrahim, *J. Inorg. Organomet. Polym. Mater.*, 2020, **30**, 2182–2196.

29 E. A. Abdelrahman, Y. G. Abou El-Reash, H. M. Youssef, Y. H. Kotp and R. M. Hegazey, *J. Hazard. Mater.*, 2021, **401**, 123813.

30 E. C. Paris, J. O. D. Malafatti, H. C. Musetti, A. Manzoli, A. Zenatti and M. T. Escote, *Chin. J. Chem. Eng.*, 2020, **28**, 1884–1890.

31 A. Bahiraei and J. Behin, *J. Environ. Chem. Eng.*, 2020, **8**, 103790.

32 A. Mohseni-Bandpi, T. J. Al-Musawi, E. Ghahramani, M. Zarrabi, S. Mohebi and S. A. Vahed, *J. Mol. Liq.*, 2016, **218**, 615–624.

33 A. S. Al-Wasidi, A. A. Almehizia, A. M. Naglah, H. M. Alkahtani, F. K. Algethami, E. S. Al-Farraj, M. T. Basha and E. A. Abdelrahman, *Int. J. Environ. Anal. Chem.*, 2022, DOI: 10.1080/03067319.2022.2153044.

34 A. A. Almehizia, M. A. Al-Omar, A. M. Naglah, R. M. Hegazey, A. S. Al-Wasidi, H. A. Katouah, M. T. Basha, R. M. Alghanmi, A. M. Khedr, F. K. Algethami and E. A. Abdelrahman, *Int. J. Environ. Anal. Chem.*, 2022, DOI: 10.1080/03067319.2022.2121164.

35 E. A. Abdelrahman and E. S. Al-Farraj, *Nanomaterials*, 2022, **12**, 3992.

36 Y. Wu and X. Wang, *Mater. Lett.*, 2011, **65**, 2062–2065.

37 M. Ranjeh, F. Beshkar, O. Amiri, M. Salavati-Niasari and H. Moayedi, *J. Alloys Compd.*, 2020, **815**, 152451.

38 R. Del Toro, P. Hernández, Y. Díaz and J. L. Brito, *Mater. Lett.*, 2013, **107**, 231–234.

39 S. Bayat, D. Ghanbari and M. Salavati-Niasari, *J. Mol. Liq.*, 2016, **220**, 223–231.

40 M. Chrunik, A. Majchrowski, D. Zasada, A. Chlanda, M. Szala and M. Salerno, *J. Alloys Compd.*, 2017, **725**, 587–597.

41 Q. Wang, Q. Chang, Y. Wang, X. Wang and J. E. Zhou, *Mater. Lett.*, 2016, **173**, 64–67.

42 R. Mohassel, A. Sobhani, M. Salavati-Niasari and M. Goudarzi, *Spectrochim. Acta, Part A*, 2018, **204**, 232–240.

43 G. Patrinoiu, J. R. Rodriguez, Y. Wang, R. Birjega, P. Osiceanu, A. M. Musuc, Z. Qi, H. Wang, V. G. Pol, J. M. Calderon-Moreno and O. Carp, *Appl. Surf. Sci.*, 2020, **510**, 145431.

44 J. Bhagwan, N. Kumar and Y. Sharma, *J. Energy Storage*, 2022, **46**, 103894.

45 E. A. Abdelrahman and R. M. Hegazey, *J. Inorg. Organomet. Polym. Mater.*, 2019, **29**, 346–358.

46 E. A. Abdelrahman, R. M. Hegazey and A. Alharbi, *J. Inorg. Organomet. Polym. Mater.*, 2020, **30**, 1369–1383.

47 A. Alharbi and E. A. Abdelrahman, *Spectrochim. Acta, Part A*, 2020, **226**, 117612.

48 R. M. Hegazey, E. A. Abdelrahman, Y. H. Kotp, A. M. Hameed and A. Subaihi, *J. Mater. Res. Technol.*, 2020, **9**, 1652–1661.

49 A. Subaihi, M. Morad, A. M. Hameed, A. Alharbi, Y. G. Abou El-Reash, F. K. Algethami, R. M. Hegazey and E. A. Abdelrahman, *Int. J. Environ. Anal. Chem.*, 2020, 1–12.

50 R. Mirzajani and S. Karimi, *Ultrason. Sonochem.*, 2019, **50**, 239–250.

51 A. C. De Lima Barizão, M. F. Silva, M. Andrade, F. C. Brito, R. G. Gomes and R. Bergamasco, *J. Environ. Chem. Eng.*, 2020, **8**, 103618.

52 V. Srivastava, P. Maydannik, Y. C. Sharma and M. Sillanpää, *RSC Adv.*, 2015, **5**, 80829–80843.

53 E. Sharifpour, P. Arabkhani, F. Sadegh, A. Mousavizadeh and A. Asfaram, *Sci. Rep.*, 2022, **12**, 1–20.